Engineering of head-mounted projective displays

Hong Hua, Axelle Girardot, Chunyu Gao, and Jannick P. Rolland

Head-mounted projective displays (HMPD's) are a novel type of head-mounted display. A HMPD consists of a miniature projection lens mounted upon the user's head and retroreflective sheeting material placed strategically in the environment. First, the imaging concept of a HMPD is reviewed and its potential advantages and disadvantages are discussed. The design and a bench prototype implementation are then presented. Finally, the effects of retroreflective materials on the imaging properties and the optical properties of HMPD's are comprehensively investigated. © 2000 Optical Society of America

OCIS codes: 080.2740, 120.2040, 120.2820, 120.3620, 120.4570, 220.0220, 230.3990.

1. Introduction

Three-dimensional (3D) visualization devices such as head-mounted displays (HMD's) and projection-based displays have received considerable attention and investigation because of their potential to harmonize human–computer interaction and enhance user performance. The applications of these visualization devices span the fields of scientific 3D visualization, interactive control, education and training, telemanipulation, telepresence, wearable computers, and entertainment systems.

Immersive HMD's, represented conceptually in Fig. 1(a), block a user's real-world view to present him with a view that is under the full control of computers and to make him believe that he is part of the virtual environment.[1] This approach eliminates the possibility of using the wealth of information that exists in the real world but is difficult to duplicate with computer-graphics technology.

A promising related technology is that of see-through HMD's (STHMD's), which optically superimpose virtual objects upon an existing scene to enhance rather than replace the real scene. In this case, additional information is provided, so the user's visual system suspends disbelief and he or she perceives the computer-generated virtual objects as part of the real environment. The fusion of real and virtual images into a single scene presents new technical challenges for HMD designers.

Video-based fusion and optical-based fusion are two basic approaches to combining real and virtual images. With a video STHMD, the real-world view is captured with two miniature video cameras mounted on the top of the user's headgear.[2] Each of the two cameras takes one image of the real world for one eye; then the graphics system electronically combines the real images with the graphic images to generate the combined environment. With an optical STHMD, the real world is viewed through beam splitters placed at 45° in front of the user's eyes.[3] The mirrors also reflect the virtual images into the user's eyes, thereby optically combining real and virtual world views. A comprehensive discussion of trade-offs between optical and video STHMD's with respect to technological and human factor issues was given by Rolland and Fuchs.[4] Optical see-through, shown conceptually in Fig. 1(b), creates less intrusion into the real scene than does a video see-through approach. The challenges posed for the technology are to minimize occlusion contradiction between virtual and real objects (discussed in Subsection 5.A below), to provide images that can be displayed on a potentially bright background, and to achieve highly accurate registration of real and virtual objects.

Projection-based displays, such as the CAVE (cave automatic virtual environment), use several back-projection screens in a room and multiple head projectors to generate a multiple-user virtual space.[5] Such systems are intrinsically limited in their frame rate capability because the image generation must be time multiplexed to generate multiple-user viewpoints. Furthermore, if multiple users share the

When this study was made, the authors were with the School of Optics, Center for Research and Education in Optics and Lasers, University of Central Florida, Orlando, Florida 32816. H. Hua is now with the Beckman Institute, University of Illinois, Urbana–Champaign, Illinois 61801. A. Girardot is a student at l'Ecole Supérieure d'Optique, Orsay, France. J. P. Rolland's e-mail address is rolland@creol.ucf.edu.

Received 14 December 1999; revised manuscript received 9 March 2000.

0003-6935/00/220001-11$15.00/0

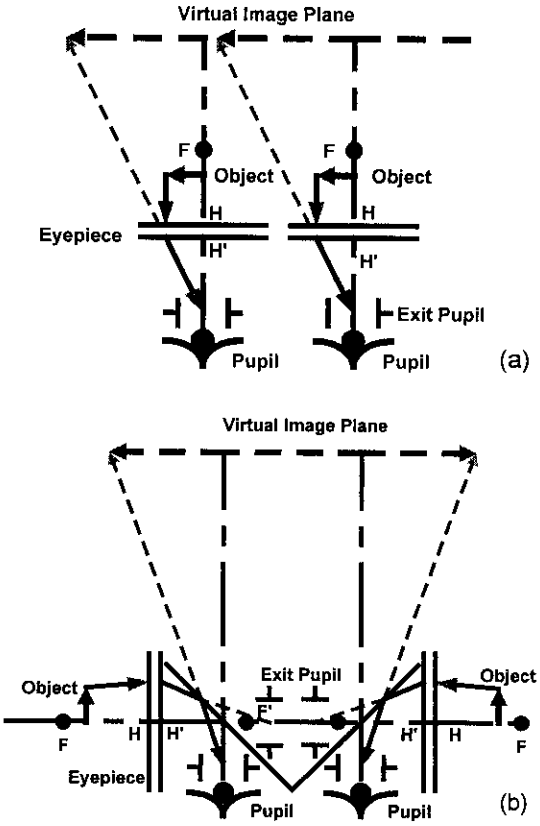

Fig. 1. Imaging concept of conventional HMD's: (a) immersive HMD, (b) optical STHMD.

same projection space, cross talk exists between them, and, as a result, only one user typically leads the collaborative team to determine the viewpoint. Finally, off-axis projection with respect to a user's viewpoint can result in keystoning, i.e., warping of the image that cannot be compensated for in the situation discussed.

A head-mounted projective display (HMPD) coupled with a supple, nondistorting, and durable projection surface is proposed as an alternative to remote displays, STHMD's, and stereo projection systems.[6,7] The imaging concept of a HMPD and its potential advantages and disadvantages are discussed first. Then the design as well as a bench prototype implementation and 3D optomechanical modeling is given. The effects of retroreflective materials on the imaging properties as well as on the optical properties of HMPD's are comprehensively investigated.

2. Concept of Head-Mounted Projection Displays

The imaging concept of HMPD's was patented by Fergason in 1997.[8] It is illustrated in Fig. 2. The final image is at least 250 mm away from the eyes to allow the user to accommodate. The HMPD components are not drawn to scale in the figure to allow for illustration of the entire system. In HMPD's, a projection lens is used instead of the eyepiece that is found in conventional HMD's. Furthermore, a retroreflective screen is used instead of the diffusing

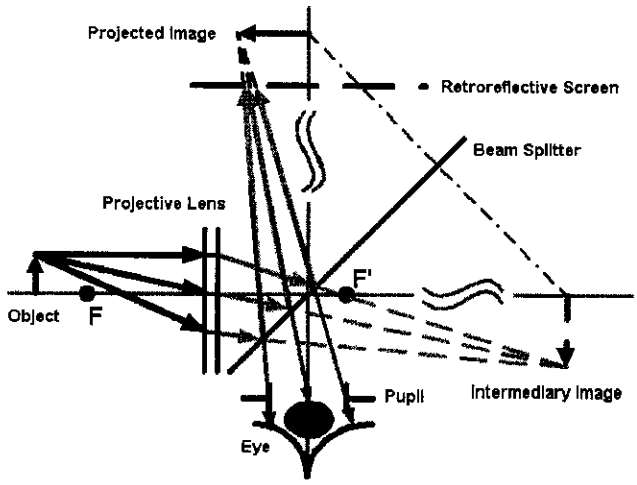

Fig. 2. Imaging concept of HMPD's.

projection screen employed by projection systems. A miniature display, located beyond the focal point of the lens instead of between the lens and the focal point as it is in conventional HMD's, serves to display computer-generated images. Through the projection lens, an intermediate image is formed. A beam splitter is placed after the projection lens at 45° with respect to the optical axis to bend the rays at 90°, as is done in an optical STHMD, but the attitude of the beam splitter is perpendicular to that of an optical STHMD. Meanwhile, a retroreflective screen is located on either side of the projected image. Because of the special characteristics of retroreflective materials, the rays hitting the surface are reflected back upon themselves in the opposite direction toward the eye of the user. At the exit pupil of the optics, a HMPD user can perceive a synthetic environment composed of virtual objects and real objects between himself and the retroreflective screen. Ideally, the location of a virtual object is independent of the location of the retroreflective screen. Moreover, the retroreflective property is independent of the incident angle. The differences among a diffusing surface, a mirror surface, and a retroreflective surface are illustrated in Fig. 3.

Given the focal length f of the projection lens, the position and size of the projected image can be calculated. With binocular HMPD's the same imaging scheme is applied to each eye. Because an ideal re-

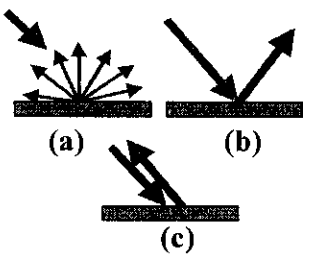

Fig. 3. Behavior of reflective surfaces: (a) diffusing surface, (b) reflective surface, (c) retroreflective surface.

Table 1. Optical Specifications of the Bench Prototype

Parameter	Measurement
Display	
Active display area	27 mm horizontal × 20 mm vertical
Pixel resolution	(640 × 3) × 480
Pixel size	0.042 mm
Mode	Color, VGA
Projection lens	
Effective focal length	22.2 mm
Field of view	50° horizontal × 42° vertical
Exit pupil diameter	10 mm
Mechanical length	35 mm long × 43 mm deep

troreflective screen does not affect the image's size and position, the size and position of the retroreflected image are the same as those of the projected image.

The advantage of using a projection lens associated with a retroreflective screen is that this configuration affords the user the ability to achieve correct occlusion of virtual objects, as discussed in Subsection 5.A below, as well as ensuring that the image brightness does not conflict with background light. For real-time graphics, a projection lens also makes it easier to correct optical distortion and other aberrations than with systems based on eyepiece design, an important property that is critical and is discussed further in Section 5. Finally, the retroreflectivity property contributes to the fact that bending the screen does not induce additional distortion (i.e., warping) of the perceived images as a result of projection onto a curved surface.[9]

3. Design Implementation

For techniques developed in our laboratory that are directed at real-time applications such as multiple-user collaboration, a mono or stereo configuration can be implemented. To investigate the imaging property of HMPD's we built a bench prototype based on a backlit liquid-crystal display in a monocular configuration. A miniature color-active matrix liquid-crystal display was used as the display device in the prototype. Of the optical components, only a projection lens needs to be custom designed, and thus we shall present the detailed layout design and performance only of the lens. The complete system layout is presented in Fig. 2, in which the lens is represented by its principal planes. The first-generation projection lens was custom designed with a double-Gauss lens form and optimized to be built from catalog lenses.[10] The optical parameters are listed in Table 1, and the optical design profile, modulation transfer function (MTF) performance, mechanical assembly, and 3D optomechanical modeling are shown in Fig. 4. A discussion of optomechanical characteristics of the HMPD was provided by Hua *et al.*[11] An image photographed from the exit pupil of the bench prototype is shown in Fig. 5. The display is a color display, but the color picture is printed in black and white in this

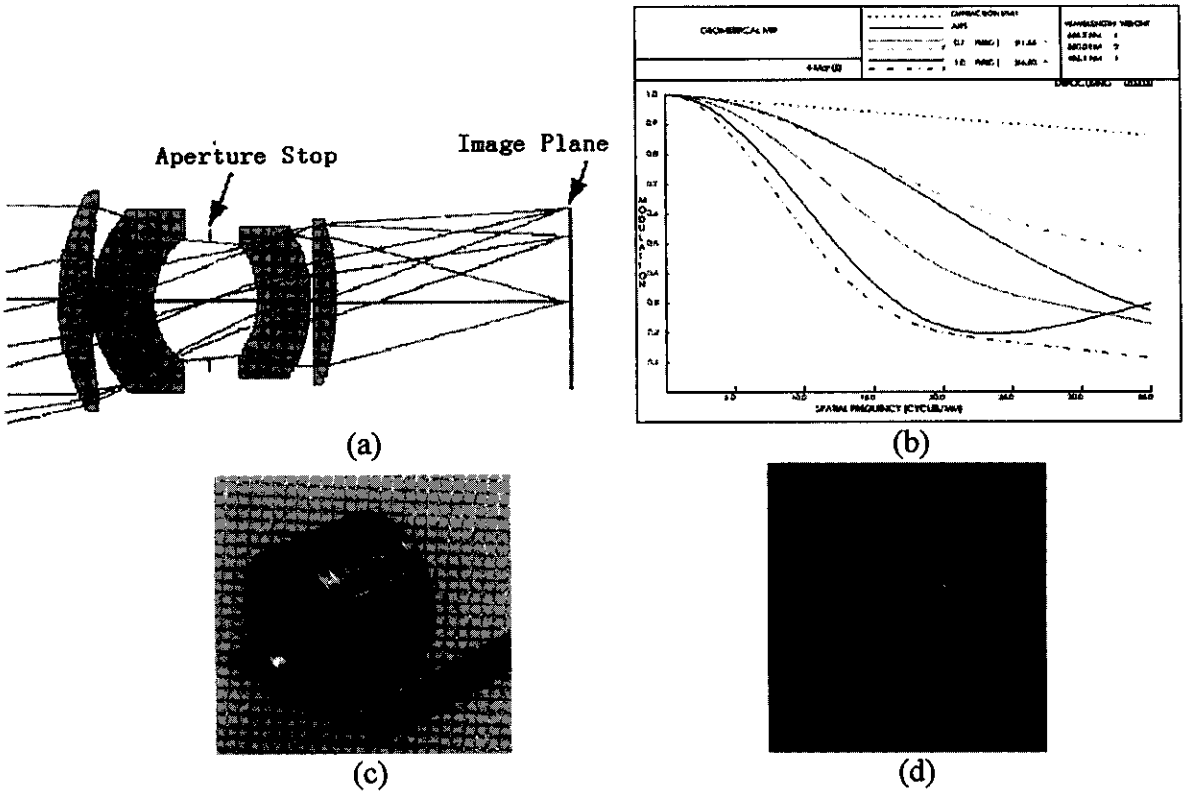

Fig. 4. Optical layout, performance, and optomechanical design. (a) optical layout, (b) MTF of the designed optics, (c) mechanical assembly, (d) 3D optomechanical modeling.

Fig. 5. Image from the bench prototype (original in color).

paper. The image viewed through the prototype is brighter and more uniform than the picture shown in Fig. 5 because of the difficulty in matching the pupil of the camera with that of the HMPD optics.

Although image quality is necessarily a function of the MTF of the projection lens, the quality and properties of the retroreflective material are also critical to the overall image quality. The retroreflective screen material is durable and bendable, with optical properties that theoretically permit undistorted two-dimensional or 3D viewing of virtual objects, regardless of the shape of the underlying projection surface. The retroreflective surface is covered with thousands of micro–corner cubes or micro-beads—approximately 47,000/in.^{2} (18500/cm^2). This type of material, commonly available from 3M or Reflexite, Inc., is routinely used in photoelectronic process control. We now describe the overall imaging properties of a screen made from micro–corner cubes or micro-beads.

4. Investigation of the Optical Properties of Several Retroreflective Materials

Two kinds of retroreflective material, micro-beads and micro–corner-cube arrays, are commercially available. Micro-bead arrays utilize specular reflection, whereas micro–corner-cube arrays utilize total internal reflection. Generally, the available retroreflective sheeting materials are optimized not for imaging optics but for traffic-control and safety applications. Furthermore, they are relied on to redirect the light shinning onto a traffic sign from a vehicle's headlights back to the driver. Therefore the rays are reflected at an angle with respect to the incident rays, instead of onto themselves. Furthermore, to account for a range of differences between vehicles, the light rays are returned in a cone, instead of in a single direction, with virtually all the reflected rays within 3° of the source. The cone reflection indicates nondirective behavior. The amount of light returned depends on the geometry of the situation and the retroreflective properties of the materials that are used. Now, after defining a few terms related to retroreflective materials, we point to their different properties as observed from experiments.

A. Definitions

Three angles are most commonly used in describing the performance of retroreflective materials in the traffic control industry; they are the entrance angle, the observation angle, and the cone angle (see, e.g., www.mmm.com/scotchlite). Entrance angle ω_e, shown in Fig. 6(a), is defined as the angle of incidence to the surface. For a HMPD, the entrance angle is linked to the field of view (FOV) of the imaging lens.

Observation angle ω_o, shown in Fig. 6(b), is defined as the angle between the incident ray and the ray reflected by the surface. For a HMPD, the observation angle is linked to image magnification at various observation distances.

Cone angle $\Delta\omega_o$, shown in Fig. 6(c), is defined as the angle range of the reflected rays about the theoretical reflected ray related to the observation angle. For a HMPD, the cone angle is linked to image blurring.

B. Measurement of the Entrance Angle

We investigated four samples of commercially available retroreflective material. Their microscopic structures are shown in Fig. 7. One is based on micro-bead structure, and the others are based on various micro–corner-cube structures. They are designated samples (a) and (b)–(d), respectively. The size of a microstructure is ~80 μm.

By using the setup shown in Fig. 8(a) we measured the retroreflectivities of the samples. A laser was used as a light source. As we tilted the retroreflective screen, we used a powermeter to record the retroreflected energy in the form of average power levels at various incident angles. Results are shown in Fig. 8(b), where the power is plotted in microwatts as a function of the incident angle. The retroreflected

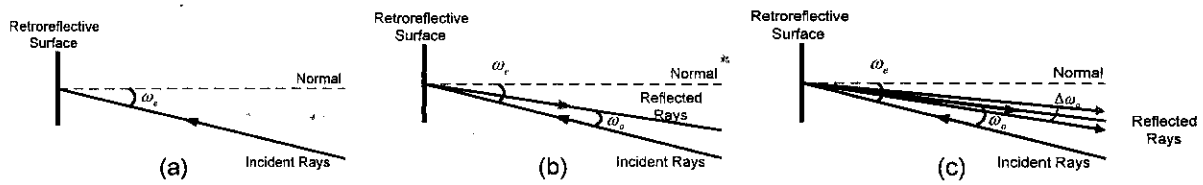

Fig. 6. Definition of entrance and observation angles of retroreflective materials: (a) entrance angle, (b) observation angle, (c) cone angle.

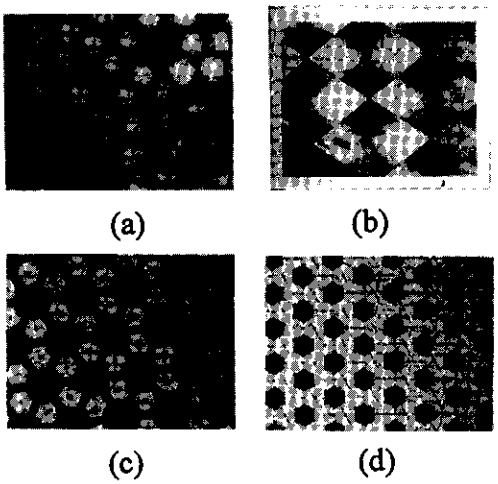

Fig. 7. Microstructure of retroreflective samples.

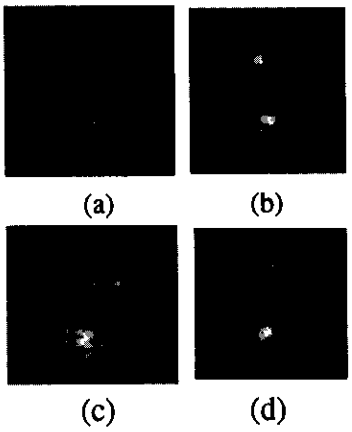

Fig. 9. Imaging properties of retroreflective samples (a)–(d) of Fig. 7.

power of the micro-bead sample is significantly less than that of the other samples, as expected, because the micro-bead sample is based on specular reflection instead of on total internal reflection.

The image power is fairly constant for a tilted angle in a range of ±40°. This indicates that, for a fairly broad range of angles, the samples behave mainly as retroreflective materials. The angle range corresponds to the range of allowable entrance angles, which implies an upper bound on the FOV of the projection lens.

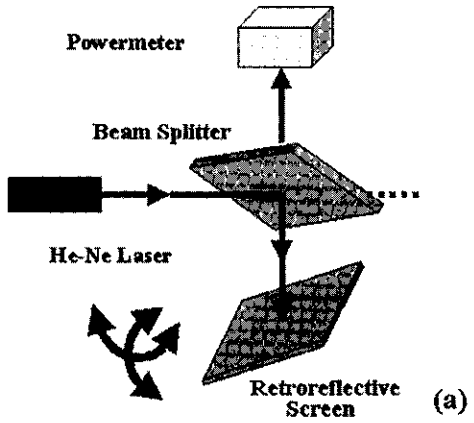

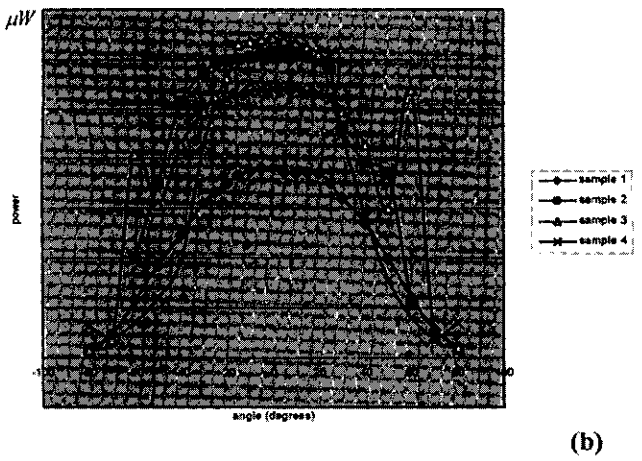

Fig. 8. Measurement of entrance angles of four samples: (a) measurement setup, (b) entrance angles.

With a setup similar to that shown in Fig. 8(a), we also observed the imaging properties of the four samples when the powermeter was replaced by a CCD camera. Results are shown in Fig. 9. We observed two essential practical challenges for optical imaging: the formation of a ghost image and the presence of artifact patterns as a result of the diffraction of the microstructures. We should point out that the speckle created by the laser source did not represent a problem in the measurements, given that only average powers were considered.

In each picture in Fig. 9 the brighter spot is the expected image and the other spot is a ghost image. This ghost image can be identified easily because it follows the screen's movement. We inferred that the ghost image is caused by the first surface of the retroreflective screen acting as a mirrored surface. A detailed analysis of ghost images is given in Section 5 below.

One way to minimize ghost images is to apply antireflective coating. Another solution is to use microstructures made from micromirrors, instead of microprisms. Such solutions suppress ghost images entirely, and we adopted one of them in our most recent systems. Because such structures are open, however, they are more prone to degradation as a result of handling and environmental factors.

C. Effects of a Nonzero Observation Angle on Imaging Properties

Even though the observation angle of the sheeting material is generally small (3° or less), it does affect the imaging properties of HMPD's. Specifically, using the bench prototype, we observed a noticeable variation in the perceived size of the reflected image, a shift of the exit pupil position of the projection lens as a function of the distance from the exit pupil of the lens

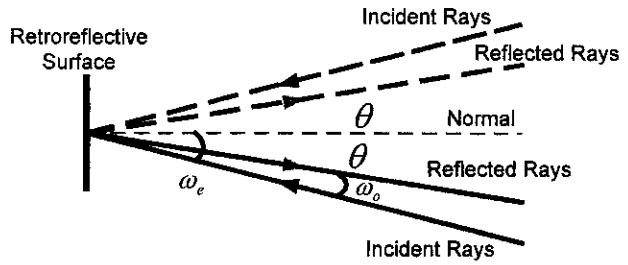

Fig. 10. Illustration of sign assumption in terms of how reflected rays are situated with respect to the incident rays.

to the reflective screen, and image blurring. These characteristics were related to the observation angle.

To quantify the effects of a nonzero observation angle we concentrate on ray tracing after the beam splitter. We define the mirror image of the exit pupil of the projection lens through the beam splitter as the entrance pupil and the image of the mirror-image pupil through the retroreflective screen as the exit pupil. We denote the diameter of the entrance pupil D_e, the diameter of the exit pupil where a user's eye is expected to be located D_x, the distance of the entrance pupil to the screen l, and the shift between the entrance and the exit pupils l_{eo}.

1. *Assumptions*

The analysis of nonzero observation angle is based on two assumptions. First, we assume that, within a certain range of entrance angles, the observation angle ω_o of the sheeting materials is a linear function of the entrance angle ω_e. Meanwhile, we also assume that when the entrance angle is zero the observation angle is zero. Second, based on the data sheets of commercially available materials used for the traffic-control industry, we assume that the reflected rays always come between the normal to the surface and the incident rays, as illustrated in Fig. 10.

If we define θ as the angle between the reflected ray and the normal to the screen surface, we then have

$$\omega_o = a\omega_e, \qquad \theta = c\omega_e, \tag{1}$$

where a is the retroreflected coefficient and $c = 1 - a$, with $0 \le c \le 1$. Ideally, $a = 0$.

2. *Analysis*

A ray tracing of the effect of a nonzero observation angle on imaging properties is shown in Fig. 11. We denote the distance between the entrance pupil and the projected image L, the distance between the exit pupil and the perceived image L', the height of the projected image H, and the perceived height of the image after the screen H'. Rays 0, 1, and 2 represent the chief, the upper, and the lower rays, respectively. The respective entrance angles on the screen, ω_{e0}, ω_{e1}, and ω_{e2}, are given by

$$\tan \omega_{e0} = \frac{H}{L},$$

$$\tan \omega_{e1} = \frac{H - R_e}{L},$$

$$\tan \omega_{e2} = \frac{H + R_e}{L}, \tag{2}$$

where $R_e = D_e/2$. According to our assumptions, rays 0, 1, and 2 are bounced back by the screen surface at angles $c\omega_{e0}$, $c\omega_{e1}$, and $c\omega_{e2}$, respectively. The exit-pupil diameter D_x and the pupil shift l_{eo} are then given by

$$D_x = D_e\left(1 - \frac{l}{L}\right) + \frac{2lH}{L}\left[1 - \frac{\tan c\omega_{e1}}{\tan c\omega_{e0}}\right],$$

$$l_{eo} = \frac{l[\tan \omega_{e0} - \tan(c\omega_{e0})]}{\tan(c\omega_{e0})}. \tag{3}$$

The perceived height of the reflected image, H', is then given by Eq. (4); the difference between H' and the height of the projected image site is given by Eq. (5):

$$H' = \frac{R_x \tan(c\omega_{e0})}{\tan(c\omega_{e0}) - \tan(c\omega_{e1})} = L' \tan(c\omega_{e0}), \tag{4}$$

$$\Delta H = \frac{R_e \tan \omega_{e0}}{\tan \omega_{e0} - \tan \omega_{e1}} - \frac{R_x \tan(c\omega_{e0})}{\tan(c\omega_{e0}) - \tan(c\omega_{e1})}$$
$$= L \tan \omega_{e0} - L' \tan(c\omega_{e0}), \tag{5}$$

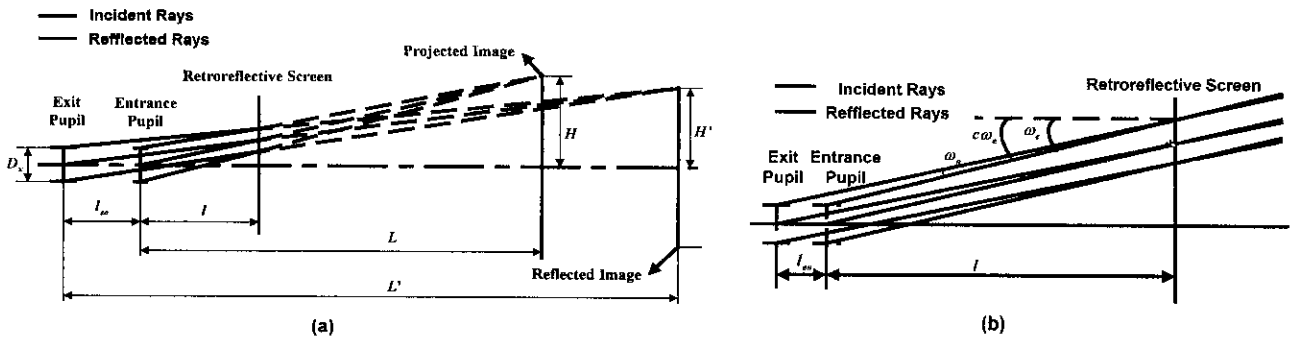

Fig. 11. Effects of observation angle: (a) noncollimated image, (b) collimated image.

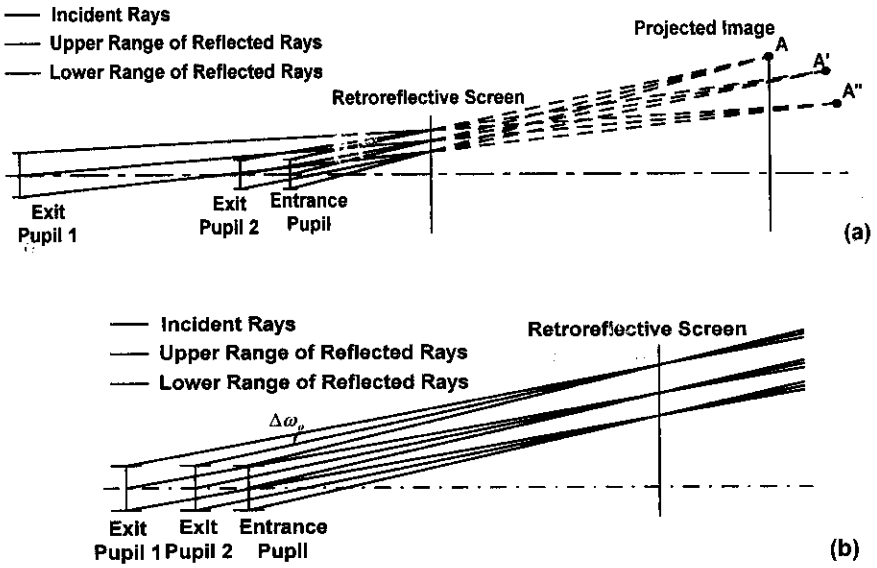

Fig. 12. Effects of cone angle: (a) noncollimated image, (b) collimated image.

where

$$L = \frac{R_e}{\tan \omega_{e0} - \tan \omega_{e1}},$$

$$L' = \frac{R_x}{\tan(c\omega_{e0}) - \tan(c\omega_{e1})},$$

$$R_x = D_x/2.$$

The difference ΔL between the perceived depth of the reflected image and that of the projected image is given by

$$\Delta L = \frac{R_e}{\tan \omega_{e0} - \tan \omega_{e1}} - \frac{R_x}{\tan(c\omega_{e0}) - \tan(c\omega_{e1})}. \quad (6)$$

In particular, if the projected image is collimated with $L \to \infty$, $\omega_{e0} = \omega_{e1} = \omega_{e2} = \omega_e$ can be established, as shown in Fig. 11(b). Collimated rays at an angle ω_e are bounced back by the screen surface at an angle $c\omega_e$. The diameters of the entrance pupil and exit pupil are the same, but the exit pupil is shifted according to Eqs. (3). The perceived size y_e of the projected image on the retina and the difference Δy_e between the perceived size after the retroreflective screen and that of the projected image are given by

$$y_e = f_e \tan(c\omega_e), \qquad \Delta y_e = f_e[\tan \omega_e - \tan(c\omega_e)], \quad (7)$$

where f_e is the focal length of the eye when it is accommodating at infinity.

In summary, Eqs. (3)–(7) indicate that the perceived size and depth of the reflected image and the exit pupil's size and location depend not only on observation angle ω_0 but on projected image distance L and screen distance l. This explains the observed phenomenon that the perceived image size and depth depend on screen distance l. Meanwhile, different points of the field correspond to different observation angles, so the exit pupil's size and position change across the FOV. Considering the fact that the eye is generally fixed at a certain position, the pupil's dependence on observation angle and screen position causes vignetting of the perceived image across the field.

D. Effects of Nonzero Cone Angle on Imaging Properties

The analysis above is based on the linear property of retroreflectivity, the assumption that one ray is reflected for a given ray angle of incidence. However, a small bundle of rays is typically retroreflected by the microstructures of the screen. This property is termed nondirectivity, and the angular range of the reflected rays is termed cone angle $\Delta\omega_o$. We assume that $\Delta\omega_o$ is constant for different entrance angles.

The effect of nonzero cone angle on imaging properties is illustrated in Fig. 12. The rays from the same object point impinge upon the retroreflective screen at angles ω_{e0}, ω_{e1}, and ω_{e2} and are reflected back at center angles $c\omega_{e0}$, $c\omega_{e1}$, and $c\omega_{e2}$ with cone angle $\Delta\omega_o$. Therefore a bundle of images is formed between points A′ and A″.

The axial separation between A′ and A″ is given by

$$(\Delta L)_c = \frac{R_{A'}}{\tan(c\omega_{e0} + \Delta\omega_o/2) - \tan(c\omega_{e1} + \Delta\omega_o/2)} - \frac{R_{A''}}{\tan(c\omega_{e0} - \Delta\omega_o/2) - \tan(c\omega_{e1} - \Delta\omega_o/2)}. \quad (8)$$

The vertical separation between A′ and A″ is given by

$$(\Delta H)_c = \frac{R_{A'}\tan(c\omega_{e0} + \Delta\omega_o/2)}{\tan(c\omega_{e0} + \Delta\omega_o/2) - \tan(c\omega_{e1} + \Delta\omega_o/2)} - \frac{R_{A''}\tan(c\omega_{e0} - \Delta\omega_o/2)}{\tan(c\omega_{e0} - \Delta\omega_o/2) - \tan(c\omega_{e1} - \Delta\omega_o/2)} \approx \frac{R_x\tan(\Delta\omega_o)}{\tan(c\omega_{e0}) - \tan(c\omega_{e1})}, \quad (9)$$

where $R_{A'}$ and $R_{A''}$ are the radii of the exit pupils of A′ and A″, respectively. In particular, if the projected image is collimated with $L \to \infty$, $\omega_{e0} = \omega_{e1} = \omega_{e2} = \omega_e$ can be established, as shown in Fig. 12(b). The separation between the upper and the lower images on the retina is then given by

$$(\Delta y_e)_c = f_e[\tan(c\omega_e + \Delta\omega_o/2) - \tan(c\omega_e - \Delta\omega_o/2)] \approx f_e\tan(\Delta\omega_o). \quad (10)$$

Meanwhile, the nonzero cone angle also causes an exit-pupil shift. The quantity of the shift has a relationship to screen distance similar to that of the nonobservation angle. In summary, the nonzero cone angle is partially responsible for ghost images and vignetting across the FOV. Using the bench prototype, we observed both phenomena.

5. Properties of the Head-Mounted Projection Display

A. Depth Perception

Visual cues pertaining to depth perception in HMPD's include occlusion, stereo, accommodation, and convergence.[12,13] Occlusion, the property of closer objects to block more-distant objects, is the most important cue to depth. Moreover, it is the only depth cue for objects farther than 2 or 3 m from the observer and is extremely important when objects or the user is in motion. In conventional STHMD's it is difficult to achieve correct occlusion between virtual objects and real scenes.[3,13] In a HMPD, real objects located between the retroreflective screen and the user block projected images at that location. Thus correct occlusion is achieved for the projected objects located behind real objects. As a consequence, if a user reaches out to grasp a virtual object, virtual objects behind his or her hand disappear naturally, as would occur in the real world. If the 3D projected objects are expected to be in front of the real objects, retroreflective material must be applied to cover the real objects. It is the essential requirement of HMPD's to display virtual objects only at locations where a retroreflective material has been positioned.

The stereoscopic cue is generated by capture of stereo pairs of images according to the location of the user's eyes.[12,14] This capability is available in HMPD's as in any other HMD's. In the case of non-eye-tracking capability, an average location is assumed in the user's interpupilary distance.[15]

Changing the focus of the eye for objects located at various distances is termed accommodation.[13,16] Accommodation may be important for the long-term comfort of HMD users. However, it is not available in HMD's or in HMPD's. Methods for overcoming this limitation have been investigated.[16,17]

Convergence is a process by which the eyes turn toward each other to aim the pupils directly at an object. To avoid diplopic vision, in nature, convergence goes hand in hand with accommodation.[18] Changing the distance from an observed object leads not only to changing convergence but also to changing lens power. However, in HMD's and other artificial stereoscopic devices, fixation always takes place with respect to one plane and accommodation does not change. The separation of the two processes that are coupled in nature leads to eye fatigue.

If a 3D simulated scene is to look and seem real, it must contain these four depth cues. Emphasis on one of these cues in HMD design depends on the applications. The HMPD's proposed in this paper can achieve correct occlusion in addition to the stereoscopic cues that are also found in other HMD's. The conflict of accommodation and convergence remains a challenge in designing HMPD's as well as conventional HMD's.

B. Depth of Field

Depth of field refers to the range of distance from the detector (e.g., the eye) in which an object appears to be in focus without the need for a change in the optical power of the lens (e.g., eye accommodation). Depth of field is inversely proportional to the pupil diameter. Depth perception of the virtual objects is practically restricted by the fact that convergence and accommodation, which are naturally linked, are decoupled in most HMD's. Whereas retinal images are not always sharp, the visual system tends to tolerate blur to a point at which essential detail is obscured. This tolerance for blur extends the apparent depth of field considerably. In conventional HMD's, multifocal plane technology can be used to achieve infinite depth of field.[17]

For immersive HMD's the depth of field is that which corresponds to the visual obscuration of the virtual scene. For STHMD's the depth of field for the real scene as well as for the virtual scene must be considered. The available depth of field for the real scene alone is essentially that of the human eye with a larger pupil than that of an unaided eye, given that the pupil is often dilated because of the loss in brightness of the real scene through a semitransparent mirror.

In most applications the virtual image plane is centered on the real scene for a STHMD. Its overlapped depth of field is also centered on the real scene. The overlapped depth of field of the HMPD is more complicated. We assume that the projection image plane is centered on the real scene, that the retroreflective screen works perfectly, and that the screen always completely occludes the real scene behind it. Thus the depth of field of the real scene is always the front part of the screen, the depth of field

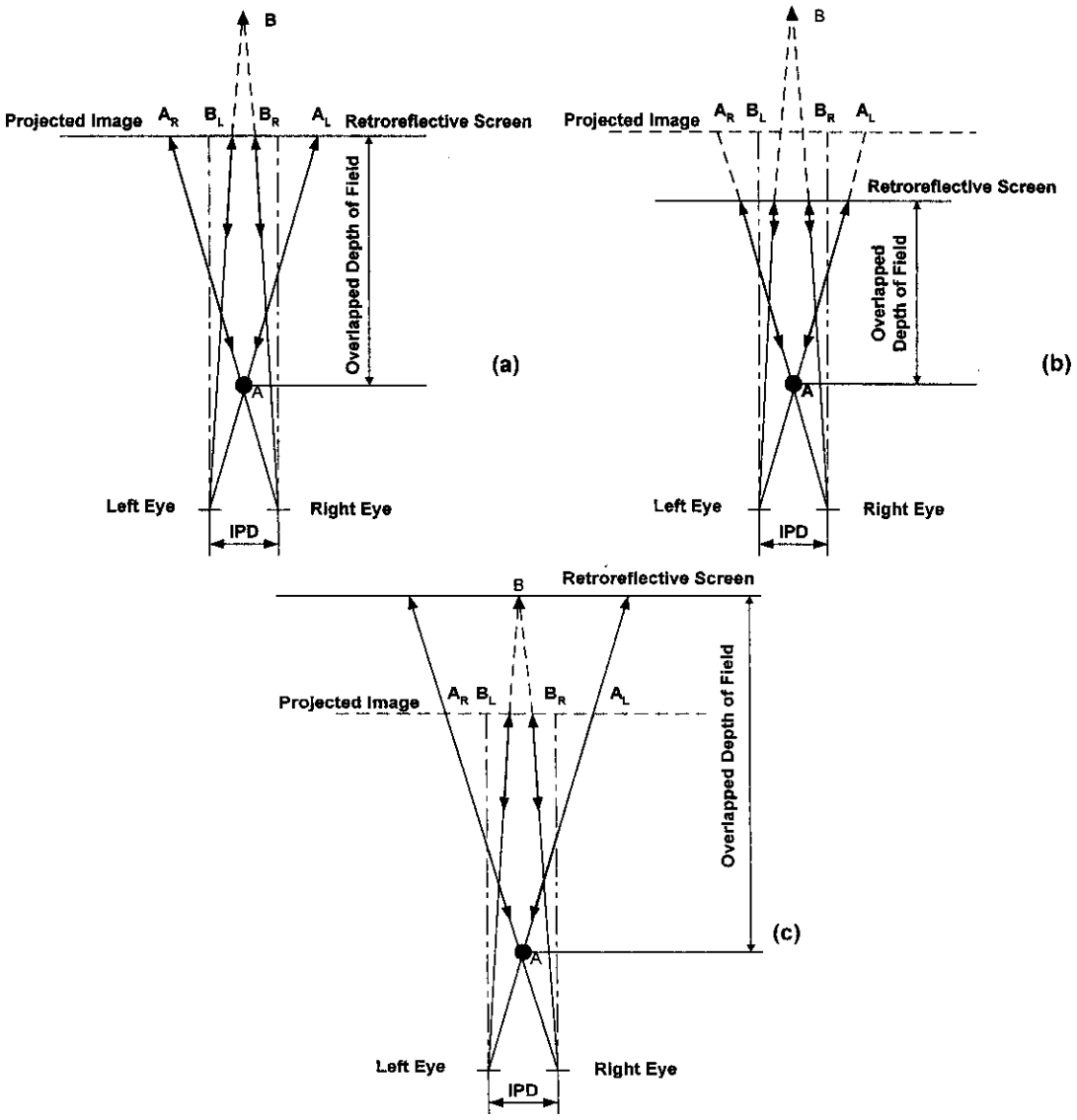

Fig. 13. Illustration of depth of field for the HMPD: (a) screen coincident with the projection plane, (b) screen in front of the projection plane, (c) screen behind the projection plane.

of the virtual scene is centered on the projection plane, and the overlapped depth of field is always between the screen and the nearest virtual objects. Furthermore, the overlapped depth of field of the HMPD can be maximized by choice of the location of the screen with respect to the projected image plane, as shown in Fig. 13. The optimized location of the screen to achieve maximum overlapped depth of field is the farthest plane of virtual objects.

C. Field of View and Resolution

Wide FOV's and high resolution are desirable properties of HMPD's as well as of HMD's, but a trade-off between the two attributes always exists because they are closely related to the focal length of the optics and to the size and resolution of the available display devices. Importantly, the FOV's of HMPD's may be limited in the upper range near 70°–80° by the range of allowable entrance angles of the retroreflective screen. New retroreflective material can be investigated for wider-FOV devices.

The vertical and horizontal FOV's, denoted $2\theta_V$ and $2\theta_H$, respectively, should meet the condition that

$$(2\theta_V, 2\theta_H) \leq 2(\omega_e)_{\max}, \tag{11}$$

where $(\omega_e)_{\max}$ is the maximum entrance angle of the reflective material.

Provided that the display resolution in pixels is $p(H) \times q(V)$ and that the size of the display is $a(H)$ mm $\times$ $b(V)$ mm, the angular resolution is given by $2\theta_H/p$ and $2\theta_V/q$ and the linear resolution is p/a and q/b for horizontal and vertical directions, respectively. In practice, it is desirable that the angular resolution be close to the angular visual acuity of the human eye (i.e., ~1 arcmin in the fovea). The linear resolution, on the other hand, imposes a line pair resolution requirement on the projection lens, which

sets a requirement on the optical design MTF performance.

D. Pupil Location and Size

In immersive HMD's an eyepiece is used for the optics. In such optics, it is required that the exit pupil be outside the eyepiece and that the eye relief distance be a minimum of 17–23 mm to provide users enough space for wearing eyeglasses. This requirement increases the difficulty of eyepiece design for HMD's. Generally, the farther the exit pupil is from the eyepiece, the more difficult it becomes to balance the optical aberrations, especially optical distortion, and the bigger and heavier the optics becomes for a given FOV. This requirement is even stronger for optical STHMD's because of the arrangement of the beam splitter typically at a $-45°$ angle from the eyepiece.

However, in HMPD's the arrangement of a beam splitter at a $+45°$ angle from the projection lens means that the beam splitter is outside the exit pupil of the projection lens and that the eye relief is equal to the distance from the beam splitter to the exit pupil of the projection lens. Therefore the exit pupil of the projection lens can be inside the lens, which indicates that the lens can be symmetrical and that optical designers can move more easily; correct optical aberrations, including optical distortion; improve the image quality provided by the optics; and keep the optics small. Such properties are highly desirable and constitute a strength of HMPD's.

The shifting of the exit pupil as a function of the distance of the reflective screen is another noticeable experimental phenomenon, which can be properly explained as being due to the observation angle of the reflective material and was analyzed in Subsection 4.D. The sheeting material must be designed with zero observation angle to minimize this imaging artifact.

E. Ghost Images

Ghost images shifted away from the desired image can cause a decrease in overall contrast, or even artifacts, and perceived blurring of the image. Assuming that the lenses that form the projection optics are coated, the main sources of ghost images are the first surface reflection of the retroreflective screen, the nondirectivity of the screen material, and the second surface reflection of the beam splitter. The nondirective effect on ghost images was analyzed in Subsection 4.D.

The retroreflectivity of the screen depends on the total internal reflection of the micro corner-cube surface. Furthermore, for materials made from micro corner-cubes the first surface of the screen works as a reflecting surface, following the specular reflection principle. In this case the ghost image formed lies beyond the FOV of the user when it is far away from the center FOV. Only within the area at the diameter of D_x do part of or all the rays from the ghost image enter the user's eye and delaminate the image quality. The axial shift of the ghost image from the expected image is given by $2\,|L - l|$.

As with conventional optical STHMD's, the second surface reflection of the beam splitter also contributes to a ghost image. The displacements of the ghost image from the desired image in both directions are

$$\frac{e}{n^2}\left(n^2 - \frac{1}{2}\right)^{1/2},$$

where e and n are the thickness and the index of the beam splitter, respectively.

6. Conclusions and Future Research

The design and implementation of a head-mounted projective display (HMPD) have been presented. The imaging concept, optical design, three-dimensional optomechanical modeling, and bench prototype implementation were provided. The effects of retroreflective materials on imaging properties were discussed comprehensively, and the imaging properties of HMPD's were investigated. The main advantages of HMPD's are that it is easier to correct optical aberrations including optical distortion in HMPD's than in conventional HMD's, their ability to project undistorted images onto curves surfaces, their potential for use in bright environments, and their ability to permit correct occlusion of real and virtual objects in virtual environments. The necessity to have a screen in the environment defines a range of applications including medical visualization and training, collaborative environments, and wearable computers.

We acknowledge the early contribution of David Poizat to the project during his internship in the Optical Diagnostics and Application (ODA) Laboratory, School of Optics, University of Central Florida, and thank Larry Davis of the ODA Lab for his stimulating comments. This research was supported by the National Institutes of Health grant 1-R29-LM06322-01A1, the Media Interface and Network Design (MIND) Laboratory, Michigan State University, and Exploration Production (ELF), Aquitaine France.

References

1. G. Burdea and P. Coiffet, *Virtual Reality Technology* (Wiley, New York, 1994).
2. A. State, G. Hirota, D. T. Chen, W. E. Garrett, and M. Livingston, "Superior augmented-reality registration by integrating landmark tracking and magnetic tracking," in *Proceedings of SIGGRAPH 96, Computer Graphic Proceedings, Annual Conference Series*, H. Rushmeier, ed. (ACM, New York, 1996), pp. 429–438.
3. J. P. Rolland, D. Ariely, and W. Gibson, "Towards quantifying depth and size perception in virtual environments," Presence: Teleoperators Virtual Environ. **4**, 24–49 (1995).
4. J. P. Rolland and H. Fuchs, "A comparison of optical and video see-through head-mounted displays," in *Fundamentals of Wearable Computers*, W. Barfield and T. Caudell, eds. (Lawrence Erlbaum & Associates, Mahwah, N. J., 2000), (to be published).
5. C. Cruz-Neira, D. J. Sandin, and T. A. DeFanti, "Surround-

screen projection-based virtual reality: the design and implementation of the CAVE," in *Proceedings of SIGGRAPH 93, Computer Graphics Proceedings, Annual Conference Series*, J. T. Kajiya, ed. (ACM, New York, 1993), pp. 135–142.
6. J. P. Rolland, J. Parsons, D. Poizat, and D. Hancock, "Conformal optics for 3D visualization," in *International Optical Design Conference 1998*, L. R. Gardner and K. P. Thompson, eds., Proc. SPIE **3482,** 760–764 (1998).
7. J. Parsons and J. P. Rolland, "A non-intrusive display technique for providing real-time data within a surgeon's critical area of interest," in *Medicine Meets Virtual Reality '98*, J. D. Westwood, H. M. Hoffman, D. Stredney, and S. J. Weghorst eds. (IOS Press, Amsterdam, The Netherlands, 1998), pp. 246–251.
8. J. Fergason, "Optical system for head mounted display using a retro-reflector and method of displaying an image," U.S. patent 5,621,572 (15 April 1997).
9. H. Hua, D. Poizat, A. Girardot, and J. P. Rolland, "Projective head-mounted displays: engineering study and design," presented at the Annual Meeting of the Optical Society of America, San Jose, Calif., 26–30 September 1999).
10. D. Poizat and J. P. Rolland, "Use of retroreflective sheets in optical system design," Tech. Rep. TR98–006 (University of Central Florida, Orlando, Fla., 1998).
11. H. Hua, A. Girardot, C. Gao, and J. P. Rolland, "Design and engineering implementation of head-mounted projective displays," presented at the Fifth Annual Conference on Human Interaction with Complex Systems, Urbana, Ill., 30 April–2 May 2000.
12. W. C. Gogel and J. D. Tietz, "Relative cues and absolute distance perception," Percept. Psychophys. **28,** 321–328 (1980).
13. J. Wann, S. Rushton, and M. Mon-Williams, "Natural problems in the perception of virtual environments," Vision Res. **35,** 2731–2736 (1995).
14. I. P. Howard and B. J. Rogers, *Binocular Vision and Steropsis*, Vol. 29 of Oxford Psychological Series (Oxford U. Press, New York, 1995).
15. J. P. Rolland, A. Yoshida, L. Davis, and J. H. Reif, "High-resolution inset head-mounted display," Appl. Opt. **37,** 4183–4193 (1998).
16. L. Marran and C. Schor, "Multiaccommodative stimuli in VR systems: problems and solutions," Hum. Factors **37,** 382–388 (1997).
17. J. P. Rolland, M. Krueger, and A. Goon, "Multifocal planes head-mounted displays," Appl. Opt. **39,** 3209–3215 (2000).
18. J. Siderov and R. S. Harwerth, "Precision of stereoscopic depth perception from double images," Vision Res. **33,** 1553–1560 (1993).